Acta Geodyn. Geomater., Vol. 17, No. 1 (197), 51–60, 2020
DOI: 10.13168/AGG.2020.0004
journal homepage: https://www.irsm.cas.cz/acta

ORIGINAL PAPER

ACOUSTIC EMISSION CHARACTERISTICS OF COAL UNDER DIFFERENT TRIAXIAL UNLOADING CONDITIONS

Yongjie YANG [1], Yan ZHOU [2] *, Depeng MA [3] *, Haiyu JI [1] and Yandong ZHANG [1]

[1] *State Key Laboratory of Mining Disaster Prevention and Control Co-founded by Shandong Province and the Ministry of Science and Technology, Shandong University of Science and Technology, Qingdao 266590, China*
[2] *Department of Resources and Civil Engineering, Shandong University of Science and Technology, Tai'an, 271019, China*
[3] *College of Water Conservancy and Civil Engineering, Shandong Agricultural University, Tai'an 271018, China*

**Corresponding author 's e-mail:* zhouyansdust@163.com and mdp123@163.com

ARTICLE INFO

Article history:
Received 18 August 2019
Accepted 16 January 2020
Available online 5 February 2020

Keywords:
Coal
Acoustic emission
Triaxial unloading
Unloading rate
Unloading confining pressure
damage

ABSTRACT

The mechanism of coal and rock damage caused by unloading during deep mining differs from that caused by continuous loading, and failure often results from a combination of loading and unloading. Triaxial unloading tests are useful for studying the damage characteristics of coal and rock under different conditions from a unloading point of view to better understand dynamic disasters of deep coal and rock. In this study, we performed triaxial tests involving loading axial stress and unloading confining pressure (4, 7, 10 MPa) using different unloading rates (0.02, 0.05, 0.08, 0.11, 0.14 MPa/s), and acoustic emission (AE) events were recorded simultaneously. The results show that the maximum AE ring and energy counting rates do not appear at peak stress but rather at the stress drop stage following peak stress. Similarly, the maximum AE impact counting rate occurs after the peak stress, which indicates that the internal cracking of the coal samples reaches a maximum at the fracture stage following peak stress. The AE information indicates a relatively quiet period prior to the occurrence of large-scale AE events. Higher initial unloading confining pressure is associated with earlier and more severe failure after peak stress. Faster unloading rates are also associated with earlier sample destruction after peak stress because the coal rapidly changes from a triaxial stress state to a uniaxial stress state with higher unloading rate, crack propagation is insufficient, and more elastic energy is released. Compared with conventional triaxial tests, the coal damage variable increases faster under triaxial unloading tests, which indicates that unloading failure is more severe.

1. INTRODUCTION

Recent years have seen a gradual depth increase of mining operations and an associated increase in the frequency and intensity of dynamic mine disasters. Coal as a complex porous medium exhibits a range of mechanical characteristics under different conditions that have an important impact on mine safety. The damage and evolution process of rocks under external loads is accompanied by signals of sound, light, electricity, heat, and magnetism, which are particularly important indicators of disaster prediction and early warning in the fields of geotechnical and mining engineering fi (Moradian et al., 2016; Rabiei et al., 2013; Chen et al., 2016; Li et al., 2020). These features play a significant role in the prediction and early warning of various kinds of engineering disasters associated with tunnel engineering, water conservancy, and hydropower engineering. The coal deformation and failure processes involve micro-crack initiation, propagation, and fracturing, and instantaneous strain energy released as an elastic waveform is termed acoustic emission (AE). AE is a nondestructive technique that has been applied and developed for more than half a century (Su et al., 2009; Aker et al., 2014; Li et al., 2010; Kang et al., 2017; Zhao et al., 2013), and changes in the nature of the rock can be deduced using AE information, as well as the failure mechanism (Davi et al., 2013).

Several previous studies have addressed AE characteristics during coal and rock deformation and damage. Since the proposal of the AE concept (Hodgson et al., 1942; Obert et al., 2013) and discovery of the Kaiser effect (Kaiser et al., 1953), AE technology has been successfully applied to managing and preventing coal mine disasters (Cao et al., 2007; Shkuratnik et al., 2004; Shkuratnik et al., 2005; Liu et al., 2007). Behnia et al. (2014) introduced common methods and advantages and disadvantages of fracture classification based on AE. Liu et al. (2007) studied the spatio-temporal evolution of tension and shear failure of granite using a matrix quantity analysis method. Ohno et al. (2010) used AE characteristic parameters and moment tensors to study the change characteristics of the tension and shear of concrete during failure. Both methods yield the same results. Several studies have also addressed fractal (Zhang et al., 2018; Ma et al.,

Cite this article as: Yang Y, Zhou Y, Ma D, Ji H, Zhang Y: Acoustic emission characteristics of coal under different triaxial unloading conditions. Acta Geodyn. Geomater., 17, No. 1 (197), 51–60, 2020. DOI: 10.13168/AGG.2020.0004

Fig. 1 Rock specimen processing procedure.

2018; Kong et al., 2016; Biancolini et al., 2009), spectral (Traore et al., 2017; Wu et al., 2018; Gong et al., 2017), and waveform characteristics (Feng et al., 2017; Wang et al., 2018) of AE signals and obtained many useful conclusions.

In previous triaxial acoustic emission tests, AE detectors have often been located on the outer wall of the triaxial chamber, which makes it difficult to obtain reliable AE information owing to the influence of mechanical vibration during signal transmission. The AE test method under triaxial conditions involving coal rock samples therefore requires further study, especially under triaxial unloading AE testing.

In addition to in-situ stress, coal mass is also affected by mining stress and deformation and failure of a coal mass often results from the combined action of loading and unloading.

For the problem of unloading failure of rock, many scholars have carried out unloading tests to study the influence of unloading on the mechanical properties of rock. For example, Qiu et al. (2010), Wang et al. (2011), Li et al. (1993) carried out different rate of unloading tests on marble, limestone and basalt respectively, through the analysis of unloading process and failure point, the effect of unloading rate on different rock mechanical characteristics was obtained, and it was also shown that the specimen would be damaged during unloading process; Huang et al. (2010) and Jiang et al. (2013) carried out respectively the unloading test of marble and rock salt focuses on the deformation and damage characteristics at the unloading end point, some rocks will be damaged at the unloading end point; Zhao et al.(2014) and He et al. (2014) have proved that rock burst may occur in the residual stage after unloading through granite unloading test. It is not difficult to find that the research on the unloading of confining pressure mainly includes the failure point, unloading end point and a characteristic point of residual stage in the unloading process of marble, limestone and other rocks. The research on the acoustic emission characteristics of coal unloading is not enough.

In engineering design, only the stability of coal and rock mass under loading conditions is considered and the influence of unloading is typically neglected, which leads to a mismatch between the design result and actual engineering. Analysis of the unloading damage and failure mechanism of coal and rock using AE monitoring techniques is therefore of great significance for obtaining coal damage and fracture characteristics under loading and unloading conditions, improved prediction accuracy of coal failure and instability, as well as improved design and construction of geotechnical engineering projects and safe mining production.

2. MATERIALS AND METHODS

2.1. STARTING MATERIAL

Coal samples were collected from the No. 16 coal seam in the Yangcun coal mine, Jining, Shandong, China. The coal block was cut into 50 × 100 mm (diameter × high) cylinders according to engineering rock mass test standards. To ensure homogeneity, samples were subjected to ultrasonic testing and specimens with high wave velocities were removed, leaving specimens with similar velocities. Coal samples used in the tests are shown in Figure 1.

2.2. EXPERIMENTAL PROCEDURE

Triaxial loading and unloading tests were performed using a MTS815.02 electro-hydraulic servo rock mechanics test system at the China University of Mining and Technology. The test system meets test requirements under a variety of complex paths. The experimental procedure is as follows.

Under loading conditions, triaxial tests were performed under different confining pressures (4, 7 or 10 MPa), which was gradually applied under hydrostatic pressure. Under constant confining pressure, the axial pressure was increased by axial displacement control at a loading rate of 0.002 mm/s until specimen failure.

The lateral stress of coal bodies (equivalent to the confining pressure) is gradually reduced during mining, and the advanced bearing pressure (equivalent to the axial stress) gradually increases. Working face mining involves a reduction of

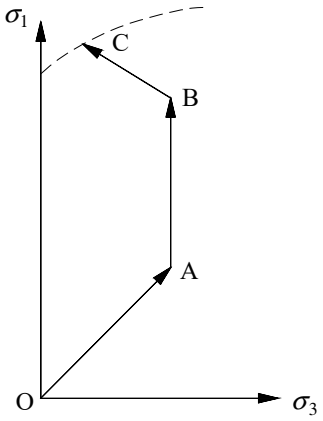

Fig. 2 Stress path of unloading confining pressure

Fig. 3 Test process and rock samples after testing.

confining pressure and increase of axial pressure of the rock mass and its surrounding rock mass. Experiments were therefore also performed under an unloading path of increasing axial pressure and unloading confining pressure. Unloading tests are more dangerous and the specimen failure time is short. The unloading experiments were divided into three stages: (1) Gradual increase of the confining pressure (σ_3) to a predetermined value (4, 7 or 10 MPa) according to the hydrostatic pressure conditions. (2) The σ_3 value is held constant while increasing the axial pressure (σ_1) to 80% of the compressive peak stress of conventional triaxial tests using the stress control method. (3) The displacement control method is used to increase σ_1 while simultaneously decreasing σ_3 at a rate of 0.02, 0.05, 0.08, 0.11 or 0.14 MPa/s until sample failure. The reduction of confining pressure stops immediately after the specimen is damaged, while axial pressure continues to load to the residual strength of the specimen using the displacement control method. The stress path of the unloading confining pressure is shown in Figure 2, and the test process and fracture rock pattern are shown in Figure 3.

Parameters of the AE equipment are set as follows. The sampling frequency is 10 MHz, the gain is 30 dB, the threshold value is 35 dB, the impact definition time is 50 μs, the impact interval time is 300 μs, and the threshold voltage is set to 1.0 V.

3. ACOUSTIC EMISSION CHARACTERISTICS OF TRIAXIAL UNLOADING TESTS

3.1. STRESS-STRAIN RELATIONSHIP

Triaxial unloading tests were carried out on a large number of coal samples under different test conditions. Figure 4 shows the stress-strain curves over the entire triaxial unloading test under different initial confining pressures and unloading rates.

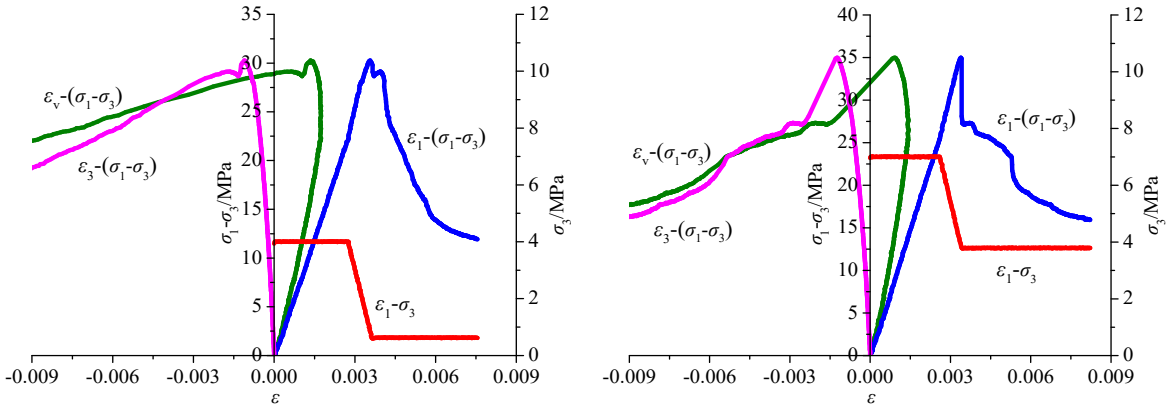

(a) C-4-0.05 (b) C-7-0.05

Fig. 4 Stress-strain curves of unloading confining pressure test of the coal samples. C represents coal, 4, 7, 10, etc. represent different initial confining pressures (MPa), and 0.02, 0.05, 0.08 etc. represent the unloading rate (MPa/s).

Table 1 Test data of different initial unloading confining pressure and unloading confining pressure rates. The variable ε_1 represents axial strain, ε_3 is circumferential strain, ε_v is volumetric strain, σ_3 is confining pressure (MPa), $v_{\sigma 3}$ is unloading rate (MPa/s), σ_1-σ_3 is principal stress difference (MPa) σ'_3 is the failure confining pressure (MPa), and σ_3-σ'_3 is the reduction of confining pressure (MPa).

Values at the peak stress								
σ_3 /MPa	$v_{\sigma 3}$ /MPa/s	σ_1-σ_3' /MPa	Residual strength /MPa	σ_3' /MPa	σ_3-σ_3' /MPa	ε_3 /mm/mm	$_1$ /mm/mm	ε_v /mm/mm
4	0.02	30.82	16.06	2.28	1.72	-0.00205	0.00462	0.00053
4	0.05	29.15	12.54	0.62	3.38	-0.00165	0.00394	0.00064
4	0.08	26.20	13.17	0.60	3.40	-0.00121	0.00372	0.00130
7	0.02	36.15	20.46	4.35	2.65	-0.00262	0.00570	-0.00034
7	0.05	34.99	19.72	3.80	3.20	-0.00173	0.00439	0.00093
7	0.08	35.20	15.60	1.61	5.39	-0.00143	0.00395	0.00060
10	0.02	50.54	24.34	6.07	3.93	-0.00285	0.00687	0.00116
10	0.05	48.75	15.68	4.53	5.47	-0.00268	0.00610	0.00074
10	0.08	43.15	17.49	4.53	5.47	-0.00228	0.00562	0.00107
10	0.11	44.10	11.33	1.55	8.45	-0.00211	0.00525	-0.00134
10	0.14	42.24	8.45	1.39	8.61	-0.00205	0.00514	0.00025

A set of the triaxial unloading test data is listed in Table 1 under different initial confining pressure and unloading rates. Brittle characteristics are apparent under different initial confining pressures and unloading rates, and brittle failure was audible during the experiments.

Upon increasing axial compression (axial loading stage) at the beginning of the test, the stress-strain curve is nearly linear except for the compaction stage. Compared with the circumferential strain, the slope of the axial strain is smaller and the increase rate of circumferential strain of coal sample is less than that of axial strain, which is similar to conventional triaxial compression. At this time, volume strain is mainly affected by axial strain.

After the start of unloading, owing to the use of displacement control for axial loading, the axial strain continues to increase at the original speed while the rate of circumferential strain increases significantly. The variation laws of volumetric strain and circumferential strain is essentially the same. As the strain curves increase, the coal sample begins to expand, which indicates that circumferential strain plays a dominant role in the confining pressure unloading stage.

As confining pressure continues to decrease, the carrying capacity of the coal samples declines, dilatation occurs, and the samples ultimately break and destabilize, resulting in crisp sound upon destruction. In the triaxial unloading tests, the restraining effect of confining pressure on the sample surface weakens with decreasing confining pressure and the destructive degree is more severe compared with that during conventional triaxial compression tests.

3.2. CHARACTERISTICS OF AE RING AND ENERGY COUNTING RATES

The relationship between AE ring and energy counting rates with experimental duration and axial strain during triaxial unloading tests is shown in Figure 5. The regularity of the AE ring counting rate and energy counting rate curves are similar for each sample during the damage and fracture stages of the coal samples. Based on the mechanism of the triaxial unloading tests, the AE ring and energy counting rates change during fracture as follows. The specific data described here are illustrated in Figure 5a.

Compaction stage (OA): Sporadic AE occurs when primary fissures close during the compaction stage. The ring counting rate is less than 10 times/s. The frequency and value are very small compared with AE information collected over the entire test process.

Elastoplastic stage (AB): Almost no AE activity occurs in the early stage of the elastoplastic stage. With the increase of axial stress, energy accumulation in coal samples gradually increases, slip friction begins in primary cracks, and AE phenomena occur, but the AE events are still relatively low overall. The ring counting rate is about 220 times/s. In the later elastoplastic stage before unloading, a large amount of energy accumulates in the coal sample, crack initiation and propagation appears, the number of AE events begins to increase significantly, and the maximum ring counting rate reaches 760 times/s. The ring and energy counting rates are several times higher than the earlier elastoplastic stage, and the AE activity enters the active stage.

Unloading and fracture stage (BD): After the beginning of unloading, the confining pressure gradually decreases and the axial load continues to increase. There are large-scale and a high number of cracks inside the coal sample and the AE activity is further enhanced with loading. As the load increases and confining pressure decreases, the AE events begin to weaken and become greatly reduced compared with the active period. There is a period of "relative silence" that lasts ~44s. After the relative quiet period, the coal sample reaches the peak stress (point C), and then enters the fracture stage. At this time, cracks in the coal sample begin to expand,

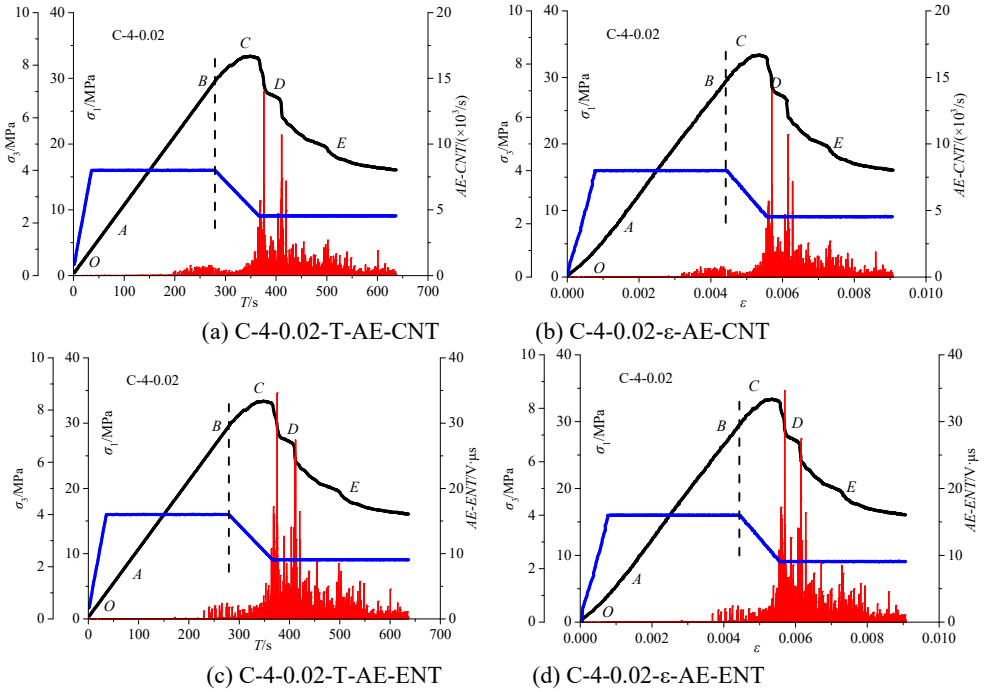

(a) C-4-0.02-T-AE-CNT (b) C-4-0.02-ε-AE-CNT

(c) C-4-0.02-T-AE-ENT (d) C-4-0.02-ε-AE-ENT

Fig. 5 Test results of AE curves of rock samples under unloading confining pressure. T and ε represent the experimental time and axial strain, respectively. AE-CNT, AE-ENT, AE-A and AE-IC represent the AE ringing counting rate, energy counting rate, amplitude, and impact counting rate, respectively. C-10-0.02-ε-AE-CNT indicates the test curve of the AE ring counting rate under a triaxial unloading test with an initial confining pressure of 10 MPa and unloading rate of 0.14 MPa/s. The abscissa axis data is the axial strain.

converge, and penetrate rapidly, and the AE events increase until the coal sample is destroyed. The AE ring and energy counting rates reach a maximum and the AE is extremely active.

Macro-fracture stage (DE): In this stage, cracks continue to develop, further converge, and penetrate to form a macro-fracture surface. At this time, the counting rates of AE ringing and energy is very high. A crushed block extrudes and is deformed under continuous loading. The sample enters the residual crushing process and the ringing count gradually decreases.

Plastic flow stage: After point E, the coal samples slip macroscopically and enter the plastic flow stage. With the development of plastic deformation, the samples loosen and further break into the residual strength stage. At this stage, the counting rates of AE ringing and energy counting are greatly reduced, and some disappear entirely at a later residual stage.

3.3. CHARACTERISTICS OF ACOUSTIC EMISSION AMPLITUDE AND IMPACT COUNTING

The distribution of AE amplitudes and impact counting rates of coal samples under triaxial unloading conditions is shown in Figure 6. The AE amplitude is widely distributed over the full test, ranging from 40 to 90 dB, owing to the development of pores and microcracks in the sample.

The development of internal pores and cracks at the beginning of the test leads to an increased range of amplitude distribution with increasing amplitude before the stress peak (40–85 dB). After the peak stress, the amplitude range reaches a maximum but narrows rapidly between 80 and 85 dB. During the residual strength stage, the distribution range increases but the amplitude decreases.

The changing curve of the AE impact counting rate shows that primary cracks are compacted under confining pressure during the axial loading stage, the internal structure of the rock sample is relatively compact, and the impact counting rate is relatively small. With increasing axial load, internal cracks begin to germinate and expand, and the impact counting rate gradually increases. After unloading, the impact counting rate increases further, reaching a maximum after the peak stress, and then decreases but at still a higher rate.

The number of cracks and rate of crack propagation can be reflected by impact counting. The maximum value of the AE impact counting rate occurs after peak stress, which indicates that internal cracks develop in the coal samples with decreasing confining pressure until failure.

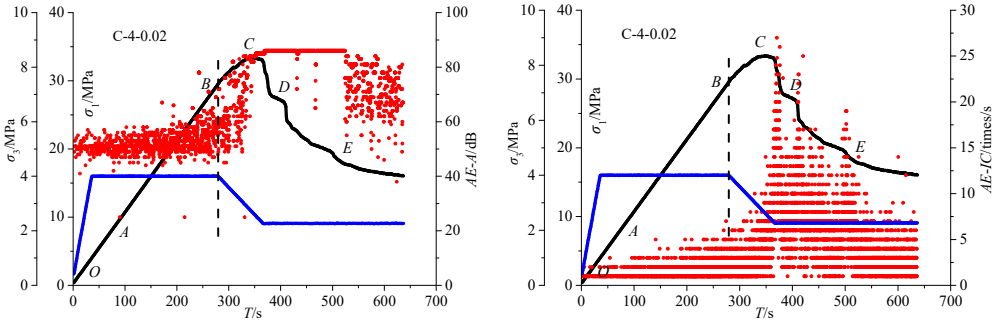

(a) C-4-0.02-*T*-AE-A (b) C-4-0.02-*T*-AE-IC

Fig. 6 Results of AE impact counts and amplitude distribution of the tested coal samples.

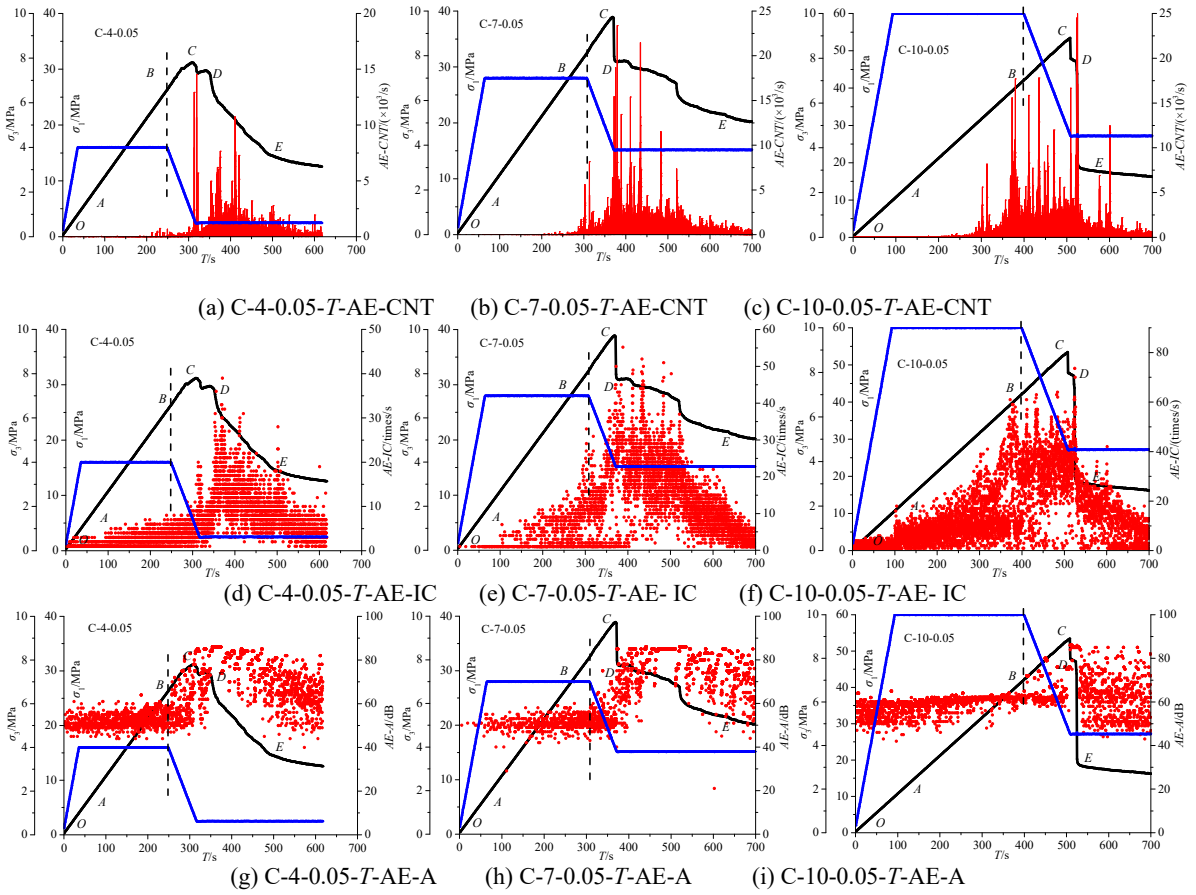

(a) C-4-0.05-*T*-AE-CNT (b) C-7-0.05-*T*-AE-CNT (c) C-10-0.05-*T*-AE-CNT

(d) C-4-0.05-*T*-AE-IC (e) C-7-0.05-*T*-AE- IC (f) C-10-0.05-*T*-AE- IC

(g) C-4-0.05-*T*-AE-A (h) C-7-0.05-*T*-AE-A (i) C-10-0.05-*T*-AE-A

Fig. 7 AE characterization parameters of coal samples under different initial confining pressure unloading.

4. ACOUSTIC EMISSION CHARACTERISTICS UNDER DIFFERENT TEST PATHS

4.1. EFFECT OF INITIAL CONFINING PRESSURE

The AE ringing counting rate, impact counting rate, and amplitude distribution of the triaxial unloading confining tests under different initial confining pressures (4, 7, 10 MPa) and fixed unloading rate (0.05 MPa/s) are shown in Figure 7. Because the distributions of the AE energy counting rate and ringing counting rate are very similar, we only discuss the ringing counting rate here.

AE characteristic parameters of coal under different initial confining pressures are listed in Table 2.

As shown in Figure 7 and Table 2, when the test enters the unloading stage, the AE ring counting rate increases significantly. After a period of time, the test enters the relative AE quiet period. At the same rate of unloading, the relative quiet period duration decreases with increasing confining pressure. When the rate is 0.05 MPa/s and the confining pressure is 4, 7 and 10 MPa, the relative quiet period duration is 34,

Table 2 AE characteristic parameters of coal samples under different initial confining pressure unloading. T_Q is the duration of the relative quiet period (s), $T_{\sigma c}$ is the time when the coal sample reaches the peak stress (s), T_{CNT}, T_{IC} and T_A are the times when the maximum value of the AE ringing counting rate, impact counting rate and amplitude appear (s), respectively, $T_{\sigma c}$-T_{CNT}, $T_{\sigma c}$-T_{IC} and $T_{\sigma c}$-T_A are the time differences between the peak stress and maximum AE parameters (s), "+" and "-" indicate that the time that AE parameters appear earlier or later than the peak stress, respectively, M_{CNT} and M_{IC} represent the maximum AE ring counting rate (times/s) and impact counting rate (times/s), respectively, and σ_Q and σ_C indicate the stress at the beginning of the relative quiet period of AE and peak stress (MPa), respectively.

σ_C/MPa	$v_{\sigma C}$/ MPa/s	T_Q/s	$T_{\sigma c}$-T_{IC}/s	$T_{\sigma c}$-T_{CNT}/s	$T_{\sigma c}$-T_A/s	σ_Q /σ_C	M_{CNT}/times	M_{IC}/times
4	0.05	34	-44	-12	-9	0.959	14530	39
7	0.05	27	-18	-10	-5	0.921	23370	55
10	0.05	22	-16	-10	-5	0.955	28360	73

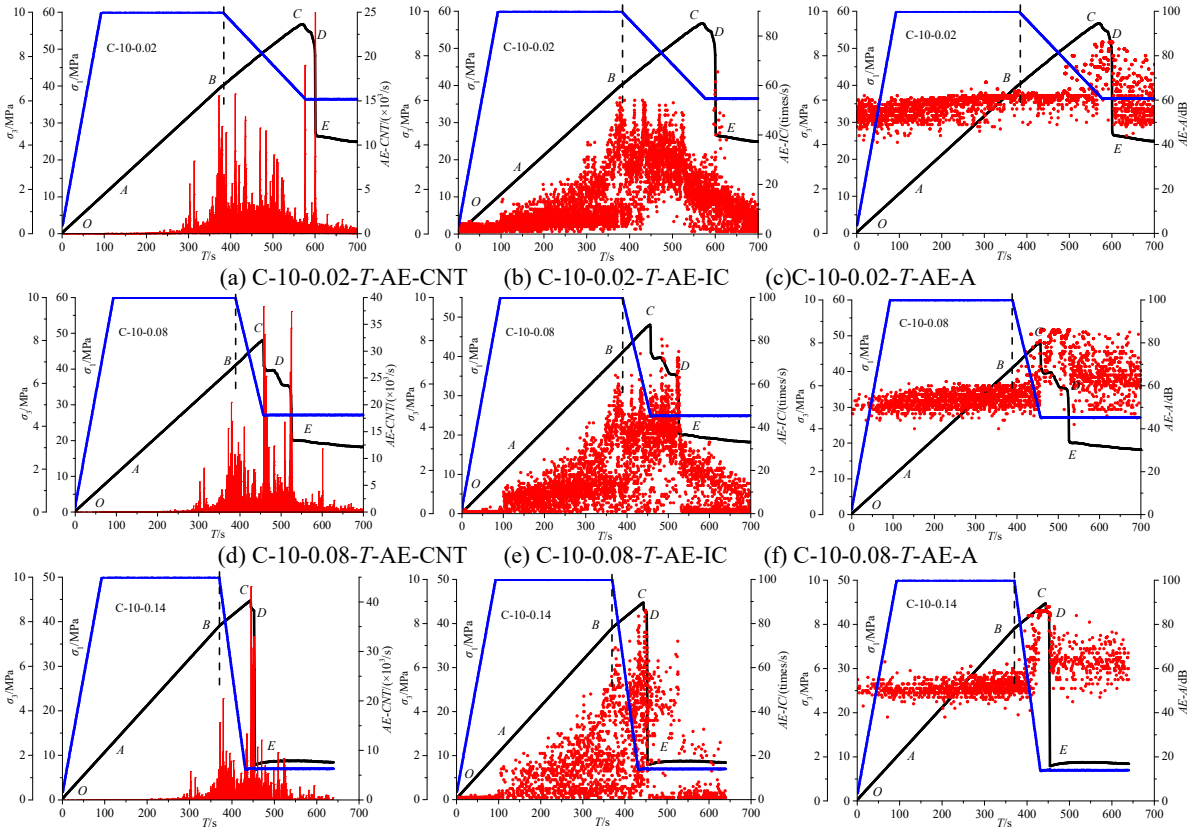

(a) C-10-0.02-*T*-AE-CNT (b) C-10-0.02-*T*-AE-IC (c)C-10-0.02-*T*-AE-A

(d) C-10-0.08-*T*-AE-CNT (e) C-10-0.08-*T*-AE-IC (f) C-10-0.08-*T*-AE-A

Fig. 8 AE characterization parameters of coal samples under different unloading confining pressure rates.

Table 3 AE parameters of coal samples under different unloading rates.

σ_C/MPa	$v_{\sigma C}$/MPa/s	T_Q/s	$T_{\sigma c}$-T_{IC}/s	$T_{\sigma c}$-T_{CNT}/s	$T_{\sigma c}$-T_A/s	σ_Q /σ_C	M_{CNT}/times	M_{IC}/times
10	0.02	34	-30	-25	-5	0.956	26340	65
10	0.05	22	-16	-10	-5	0.955	28360	73
10	0.08	21	-28	-3	-3	0.958	38300	80
10	0.11	19	-14	-3	-2	0.949	42800	82
10	0.14	17	-7	-2	-2	0.953	43100	86

27 and 22 s, respectively. The ratio of stress at the beginning of the relative quiet period to peak stress under different confining pressures is almost the same, all around 0.95. After the relative quiet period, AE activity clearly increases, the coal sample reaches the peak stress, and rupture and instability occur. The AE ring counting rate reaches a maximum, which increases with confining pressure. When the unloading rate is 0.05 MPa/s and the confining pressure is 4, 7 and 10 MPa, the maximum ringing counting rates are 14,530, 23,370 and 28,360 times/s, respectively. The values of $T_{\sigma c}$-T_{CNT} are negative, indicating that the maximum AE ringing counting rate occurs in the fracture period after peak stress.

The change laws of AE impact counting rate and amplitude are similar to that of the ringing counting rate after the start of unloading. The maximum values of impact counting rate and amplitude also occur in the fracture period after the peak stress. When the rate is 0.05 MPa/s and confining pressure is 4, 7 and 10 MPa, the maximum impact counting rate lags behind the peak stress by 39, 55, and 73 s, respectively, and the maximum amplitude lags behind the peak stress by 9, 5 and 5 s, respectively. Put simply, increased confining pressure corresponds with higher maximum impact counting rates, while the occurrence time of the maximum impact counting rate and amplitude after the peak stress gradually decrease. This shows that at the same confining pressure unloading rate, higher initial confining pressure is associated with earlier failure after the peak stress and more severe damage.

4.2. AE CHARACTERISTICS OF DIFFERENT UNLOADING RATES

Figure 8 shows the characteristics of AE ringing counts, impact counting rate, and amplitude distribution of coal samples under an initial confining pressure of 10 MPa and unloading rates of 0.02, 0.08 and 0.14 MPa/s.

Figure 8 and Table 3 show that the intensity of AE activity under different unloading rates is weak and sporadic during the initial test stage. AE activity gradually increases with increased axial loading and enters an active state during the late elastic stage. AE activity is further enhanced when the test enters the unloading stage. However, with increasing load and decreasing confining pressure, AE events begin to weaken. Compared with the active period, the AE events decrease dramatically, resulting in a “relative quiet” period. Under the same initial confining pressure, the duration of the relative quiet period decreases with increased unloading. When the initial confining pressure is 10 MPa and confining pressure rate is 0.02, 0.05, 0.08, 0.11 and 0.14 MPa/s, the relative quiet duration is 34, 22, 21, 19 and 17 s, respectively. As before, the ratio of stress at the beginning of the relative quiet period to peak stress under different unloading rates is almost the same, all around 0.95. After the relative quiet period, the AE activity clearly increases, the coal samples reach peak stress and then undergo rupture and instability. The ringing counting rate reaches a maximum, which increases with unloading rate. When the unloading rate is 0.02, 0.05, 0.08, 0.11 and 0.14 MPa/s, the maximum ringing counting rate is 26,340, 28,360, 38,300, 42,800 and 43,100 times/s, respectively. At the same time, the values of $T_{\sigma c}$-T_{CNT} are negative, which also shows that the maximum AE ringing counting rate occurs in the fracture period after peak stress under different unloading rates. Faster initial unloading rates are associated with shorter lag times. It can be concluded that under faster unloading rates, coal samples change from a triaxial state to a uniaxial state. The internal crack propagation is insufficient, more elastic energy is released than under slower unloading rates, and the coal samples are more easily destroyed.

The change laws of AE impact counting rate and amplitude are similar to that of ringing counting rate after the start of unloading but no relative quiet period is observed. The maximum impact counting rate and amplitude also occur in the fracture period after peak stress. When the unloading rate is 0.02, 0.05, 0.08, 0.11 and 0.14 MPa/s, the maximum impact counting rate lags behind the peak stress by 30, 16, 28, 14, and 7 s, respectively, the maximum impact counting rates are 65, 73, 80, 82 and 86 times/s, and the maximum amplitude lags behind the peak stress by 5, 5, 3, 2 and 2 s, respectively. In essence, increased unloading rate is associated with higher maximum impact counting rate while the time lag of the maximum occurrence after peak stress gradually decreases (except when the unloading rate is 0.08 MPa/s). This shows that under fixed confining pressure, faster unloading rates are associated with earlier failure after the peak stress and more severe damage.

5. CONCLUSIONS

1. Under conventional triaxial compression, the time when the AE ring counting rate and energy counting rate maxima occur slightly lags behind the peak stress. This can be explained by coal particle breakage and fracture slip dislocation that are restrained by confining pressure, compared with uniaxial compression, and the shear and failure strength and post-peak load-bearing capacity are improved, which results in the observed “lagging” phenomenon.
2. In triaxial unloading tests, the maximum AE impact counting rate also occurs after peak stress and the impact counts reflect the number and rate of crack propagation in the samples. This indicates that internal cracking develops with decreasing confining pressure in the unloading confining pressure stage until reaching a maximum upon sample rupture.
3. Under different initial confining pressures in the triaxial unloading tests, the maximum value of

ringing counting rate and amplitude increases with increasing initial confining pressures; however, the time lag between the maximum occurrence and peak stress decreases. This shows that higher initial unloading confining pressure is associated with earlier and more severe failure after peak stress.

4. Under different unloading rates in the triaxial unloading tests, the maximum ringing counting rate and amplitude increase with increasing unloading rate; however, the time lag when the maximum occurs after the peak stress decreases. This shows that higher unloading rates are associated with earlier failure after peak stress. It can be concluded that at higher unloading rates, coal samples change from a triaxial stress state to a uniaxial compression state in a short time, crack propagation is insufficient, more elastic energy can be released at lower unloading rates, and the coal samples are more easily destroyed.

ACKNOWLEDGMENTS

This research was funded by he National Key R&D Program of China (grant number 2018YFC0604705) and the National Natural Science Foundation of China (grant number 51574156). This research was also partially funded by the Shandong Province Higher Educational Science and Technology Program (grant number J18KA195) and the Natural Science Foundation of Shandong Province (grant number ZR2019PD016). We thank Esther Posner, PhD, from Liwen Bianji, Edanz Editing China (www.liwenbianji.cn/ac), for editing the English text of a draft of this manuscript.

REFERENCES

Aker, E., Kuhn, D., Vavrycuk, V., Soldal, M. and Oye, V.: 2014, Experimental investigation of acoustic emissions and their moment tensors in rock during failure. Int. J. Rock Mech. Min. Sci., 70, 286–295. DOI: 10.1016/j.ijrmms.2014.05.003

Behnia, A, Chai, H.K. and Shiotani, T.: 2014, Advanced structural health monitoring of concrete structures with the aid of acoustic emission. Constr. Build. Mater., 65, 282–302. DOI: 10.1016/j.conbuildmat.2014.04.103

Biancolini, M.E., Brutti, C., Paparo, G. and Zanini, A: 2006, Fatigue cracks nucleation on steel, acoustic emission and fractal analysis. Int. J. Fatigue, 28,12, 1820–1825. DOI: 10.1016/j.ijfatigue.2005.12.003

Cao, S.G., Liu, Y.B. and Zhang, L.Q.: 2007, Study on characteristics of acoustic emission in outburst coal. Chin. J. Rock Mech. Eng., 26, Suppl. 1, 2794–2799, (in Chinese).

Chen, S.J., Wang, H.L., Wang, H.Y., Guo, W.J. and Li, X.S.: 2016, Strip coal pillar design basedon estimated surface subsidence in eastern China. Rock Mech. Rock Eng., 49, 9, 3829–3838. DOI: 10.1007/s00603-016-0988-y

Davi, R., Vavrycuk, V., Charalampidou, E.M. and Kwiatek, G.: 2013, Network sensor calibration for retrieving accurate moment tensors of acoustic emissions. Int. J. Rock Mech. Min. Sci., 62, 59–67. DOI: 10.1016/j.ijrmms.2013.04.004

Feng, H.X. and Yi, W.J.: 2017, Propagation characteristics of acoustic emission wave in reinforced concrete. Results Phys., 7, 3815–3819. DOI: 10.1016/j.rinp.2017.09.060

Gong, Y.X., Song, Z.J., He, M.C. et al: 2017, Precursory waves and eigenfrequencies identified from acoustic emission data based on Singular Spectrum Analysis and laboratory rock-burst experiments. Int. J. Rock Mech. Min. Sci., 91, 155–169. DOI: 10.1016/j.ijrmms.2016.11.020

He, M.C., Zhao, F., Du, S. et al.: 2014, Rockburst characteristics based on experimental tests under different unloading rates. Rock Soil Mech., 35, 10, 2737–2747, (in Chinese).

Hodgson, E.A.: 1942, Interior of the earth viewed in its relation to earthquake causes - Viewpoint of seismology. Geol. Soc. Am. Bull., 53, 7, 1045–1053. DOI: 10.1130/GSAB-53-1045

Huang, R. and Huang, D.: 2010, Experimental research on affection laws of unloading rates on mechanical properties of Jinping marble under high geostress. Chin. J. Rock Mech. Eng., 29, 1, 21–33, (in Chinese).

Jiang, D.Y., Fan, J.Y., Chen, J. et al.: 2013, Research on effect of unloading rate of confining pressure on capacity expansion damage of salt rock. Chin. J. Rock Mech. Eng., S2, 3154–3159, (in Chinese).

Kaiser, E.J.: 1953, Knowledge and research on noise measurements during the tensile stressing of metals.

Kang, Y.M., Ni, P.P., Fu, C. and Zhang, P.H.: 2017, Estimation of damage location of rock based on denoised acoustic emission signals using wavelet packet algorithm. Geotech. Test. J., 40, 6, 963–977. DOI: 10.1520/GTJ20170029

Kong, X.G., Wang, E.Y., Hu, S.B. et al: 2016, Fractal characteristics and acoustic emission of coal containing methane in triaxial compression failure. J. Appl. Geophys., 124, 139–147. DOI: 10.1016/j.jappgeo.2015.11.018

Li, S.L. and Tang, H.Y.: 2010, Acoustic emission characteristics in failure process of rock under different uniaxial compressive loads. Chin. J. Geotech. Eng., 32, 1, 147–152, (in Chinese).

Li, T.B. and Wang, L.S.: 1993, Experimental research on deformation and failure characteristics of basalt under unloading stress condition. Chin. J. Rock Mech. Eng., 12,4, 321–327, (in Chinese).

Li, W.T., Yang, N., Mei, Y.C., Zhang, Y.H., Wang, L., Ma, H.Y.: 2020, Experimental investigation of the compression-bending property of the casing joints in a concrete filled steel tubular supporting arch for tunnel engineering. Tunn. Undergr. Sp. Tech., 96. DOI: 10.1016/j.tust.2019.103184

Liu, B.X., Zhao, B.Y. and Jiang, Y.D.: 2007, Study of deformation-damage and acoustic emission character of coal rock under uniaxial compression. Chin. J. Undergr. Space Eng., 3 ,4, 647–650, (in Chinese).

Liu, J., Li, Y., Xu, S. et al: 2015, Moment tensor analysis of acoustic emission for cracking mechanisms in rock with a pre-cut circular hole under uniaxial compression. Eng. Fract. Mech., 135, 206–218. DOI: 10.1016/j.engfracmech.2015.01.006

Ma, D.P., Zhou, Y. and Liu, Ch.X.: 2018, Creep behavior and acoustic emission characteristics of coal samples with different moisture content. Acta Geodyn. Geomater., 15, 4 ,192, 405–412. DOI: 10.13168/AGG.2018.0030

Moradian, Z., Einstein, H.H. and Ballivy, G.: 2016, Detection of cracking levels in brittle rocks by parametric analysis of the acoustic emission signals. Rock Mech. Rock Eng., 49, 3, 785–800. DOI: 10.1007/s00603-015-0775-1

Obert, L. and Duvall W.: 1942, Use of subaudible noises for the prediction of rock bursts, part II. U.S. Bur. Mines Rep. 3654.

Ohno, K. and Ohtsu, M.: 2010, Crack classification in concrete based on acoustic emission. Constr. Build. Mater., 24,12, 2339–2346. DOI: 10.1016/j.conbuildmat.2010.05.004

Qiu, S.L., Feng, X.T., Zhang, Ch.Q. et al.: 2010, Experimental research on mechanical properties of deep-buried marble under different unloading rates of confining pressures. Chin. J. Rock Mech. Eng., 29, 9, 1807–1817, (in Chinese).

Rabiei, M. and Modarres, M.: 2013, Quantitative methods for structural health management using in situ acoustic emission monitoring. Int. J. Fatigue, 49, 81–89. DOI: 10.1016/j.ijfatigue.2012.12.001

Shkuratnik, V.L., Yu, L.F. and Kuchurin, S.V.: 2004, Experimental investigations into acoustic emission in coal samples under uniaxial loading. J. Min. Sci., 40, 5, 458–464. DOI: 10.1007/s10913-005-0030-3

Shkuratnik, V.L., Yu, L.F. and Kuchurin, S.V.: 2005, Experimental regularities of acoustic emission in coal samples under triaxial compression. J. Min. Sci., 41, 1, 44–53. DOI:10.1007/s10913-005-0062-8

Su, C.D., Gao, B.B., Nan, H. and Li, X.J.: 2009, Experimental study on acoustic emission characteristics during deformation and failure processes of coal samples under different stress paths. Chin. J. Rock Mech. Eng., 28, 4, 757–766, (in Chinese).

Traore, O.I., Pantera, L., Favretto-Cristini, N., Cristini, P., Viguier-Pla, S. and Vieu, P.: 2017, Structure analysis and denoising using Singular Spectrum Analysis: Application to acoustic emission signals from nuclear safety experiments. Measurement, 104, 78–88. DOI: 10.1016/j.measurement.2017.02.019

Wang, X.R., Liu, X.D., Tai, J.F., He, T. and Shan, Y.Ch.: 2018, A novel method of reducing the acoustic emission wave reflected by boundary based on acoustic black hole. Ultrasonics, 94, 292–304. DOI: 10.1016/j.ultras.2018.08.015

Wang, Z.Q., Zhang, L.M., Sun, H. et al: 2011, Experimental study of mechanical properties of limestone under different unloading velocities. Rock Soil Mech., 32, 4, 1045–1050, (in Chinese).

Wu, X.Z., Jiang, Y.J., Guan, Z.C. and Wang, G.: 2018, Estimating the support effect of the energy-absorbing rock bolt based on the mechanical work transfer ability. Int. J. Rock Mech. Min. Sci., 103, 168–178. DOI: 10.1016/j.ijrmms.2018.01.041

Zhang, S.W., Shou, K.J., Xian, X.F. et al: 2018, Fractal characteristics and acoustic emission of anisotropic shale in Brazilian tests. Tunn. Undergr. Sp. Tech., 71, 298–308. DOI: 10.1016/j.tust.2017.08.031

Zhao, X.G., Wang, J., Cai, M. et al.: 2014, Influence of unloading rate on the strainburst characteristics of Beishan granite under true-triaxial unloading conditions. Rock Mech. Rock Eng., 47, 2, 467–483. DOI: 10.1007/s00603-013-0443-2

Zhao, Y.C., Lin, B., Tang, X.Y., Gong, Y.H., Liu, J. and Gao, Y.N.: 2013, Coal acoustic emission characteristics and damage evolution under uniaxial compression. J. Shandong Univ. (Nat. Sci.), 32, 5, 1–7, (in Chinese).